Particle export fluxes to the oxygen minimum zone of the Eastern Tropical North Atlantic

Anja Engel[1], Hannes Wagner[1], Frédéric A. C. Le Moigne[1], Samuel T. Wilson[2]

[1] GEOMAR Helmholtz Centre for Ocean Research Kiel, 24105 Kiel, Germany

[2] Daniel K. Inouye Center for Microbial Oceanography: Research and Education, Department of Oceanography, University of Hawaii, Honolulu, HI 96822, USA

Correspondence to: Anja Engel (aengel@geomar.de)

Abstract. In the ocean, sinking of particulate organic matter (POM) drives carbon export from the euphotic zone and supplies nutrition to mesopelagic communities, the feeding and degradation activities of which in turn lead to export flux attenuation. Oxygen (O_2) minimum zones (OMZs) with suboxic water layers (<5 μmol O_2 kg^{-1}) show a lower carbon flux attenuation compared to well oxygenated waters (>100 μmol O_2 kg^{-1}), supposedly due to reduced heterotrophic activity. This study focuses on sinking particle fluxes through hypoxic mesopelagic waters (<60% μmol O_2 kg^{-1}); these represent ~100 times more ocean volume globally compared to suboxic waters, but have less been studied. Particle export fluxes and attenuation coefficients were determined in the Eastern Tropical North Atlantic (ETNA) using two surface tethered drifting sediment trap arrays with 7 trapping depths located between 100 and 600m. Data on particulate matter fluxes were fitted to the normalized power function $F_z=F_{100}\ (z/100)^{-b}$, with F_{100} being the flux at a depth (z) of 100 m and *b* being the attenuation coefficient. Higher *b*-values suggest stronger flux attenuation and are influenced by factors such as faster degradation at higher temperatures. In this study, *b*-values of organic carbon fluxes varied between 0.74 and 0.80 and were in the intermediate range of previous reports, but lower than expected from seawater temperatures within the upper 500m. During this study, highest *b*-values were determined for fluxes of particulate hydrolysable amino acids (PHAA), followed by particulate organic phosphorus (POP), nitrogen (PN), carbon (POC), chlorophyll *a*, and transparent exopolymer particles (TEP), pointing to a sequential degradation of organic matter components during sinking. Our study suggests that in addition to O_2 concentration, organic matter composition co-determines transfer efficiency through the mesopelagial. The magnitude of future carbon export fluxes may therefore also depend on how organic matter quality in the surface ocean changes under influence of warming, acidification, and enhanced stratification.

1. Introduction

The biological carbon pump, defined as the export of biologically fixed carbon dioxide (CO_2) from the surface to the deeper ocean mainly in the form of sinking particles (Volk and Hoffert, 1985), influences atmospheric CO_2 concentration and affects ecosystem structure and elemental distributions in the ocean. The total amount of carbon export as well as the efficiency of the biological carbon pump, *i.e*. the ratio between export and primary production, are highly dynamic (Buesseler and Boyd, 2009; Lam et al., 2011). Changes in the efficiency of the biological carbon pump may have been responsible for past atmospheric CO_2 variability between glacial-interglacial transition periods (Kohfeld and Ridgewell, 2009) and play a key role for future climate predictions (Heinze et al., 2015).

Most of the POM being exported below the surface mixed layer (<200m in general) is solubilized and remineralized within the mesopelagic layer, *i.e*. between depths of 200 and 1000 m (Bishop et al., 1978; Suess, 1980). The shallower the carbon remineralization depth, the more likely is CO_2 to exchange with the atmosphere, and hence drive a shorter carbon storage time in the ocean (Volk and Hoffert, 1985; Kwon et al., 2009). Factors driving export flux attenuation in the mesopelagic have therefore a large influence on CO_2 sequestration in the ocean. The vertical profile of sinking particulate organic carbon (POC) flux has often been described by a normalized power function: $F_z = F_{100}(z/100)^{-b}$, where F_z is the particle flux as a function of depth z, F_{100} is the flux at 100 m depth, and b is the flux attenuation coefficient (Martin et al., 1987; hereafter *M87*). The authors of the *M87* study derived an 'open ocean composite' for POC export fluxes from North Pacific data with a F_{100} = 50.3 mg m^{-2} d^{-1} and b = 0.86. However strong regional variations of both total export POC fluxes and b values are observed (Martin et al., 1987; Buesseler et al., 2007a; Torres Valdes et al., 2014; Marsay et al., 2015) with several factors proposed to control export flux attenuation. Increased attenuation, *i.e*. higher b-values, have been related to increased temperature (Marsay et al.,

2015), zooplankton feeding activity (Lampitt et al., 1990), coprophagy, coprorhexy, and coprochaly (Belcher et al. 2016), microbial cycling (Giering et al., 2014) and lack of ballast (LeMoigne et al., 2012). Decreased flux attenuation, *i.e*. lower *b*-values, and thus higher transfer efficiencies (T_{eff}) have been associated to high particle sinking velocity depending on plankton community composition, especially the presence of larger phytoplankton cells (Buesseler, 1998; Buesseler and Boyd 2009), particle aggregates (Alldredge and Gotschalk, 1989), and fecal pellets (Cavan et al., 2015). Organic polymers, such as transparent exopolymer particles (TEP) increase the rate of aggregate formation due to their high stickiness (Alldredge et al., 1993; Engel, 2000; Passow, 2002; Chow et al., 2015) and supposedly play an important role in particle export fluxes (Passow, 2002; Arrigo, 2007; Chow et al., 2015). TEP are carbon-rich particles that form from dissolved polysaccharides (Engel et al., 2004). When included in sinking POM inventories, TEP may increase carbon relative to nitrogen export fluxes, a mechanism potentially counteracting rising CO_2 concentration in the atmosphere (Schneider et al., 2004; Arrigo, 2007; Engel et al., 2014). However, TEP themselves are non-sinking due to a high water content and low density (Azetzu-Scott and Passow, 2004), and little quantitative data are available on TEP export by sinking particles so far (Passow et al., 2000; Martin et al., 2011; Ebersbach et al., 2014). Thus, the role of TEP in carbon export is still unresolved.

Reduced POC flux attenuation has also been suggested for oxygen minimum zones (OMZs) (Martin et al., 1987; Haake et al., 1992; Devol and Hartnett, 2001; Van Mooy et al., 2002; Keil et al., 2015) as a consequence of reduced zooplankton feeding and microbial degradation activities in suboxic (<5 μmol O_2 kg^{-1}) waters. So far, the vast majority of mesopelagic downward POM flux measurements originate from well oxygenated waters (>100 μmol O_2 kg^{-1}). In the *M87* study, five sets of drifting sediment traps were deployed in the oxygenated North Pacific and four sets were deployed in the Eastern Tropical North Pacific (ETNP) OMZ. The flux attenuation coefficients (*b*) for the oxygenated North Pacific averaged 0.90 ±

106 0.06, while lower *b* values averaging 0.66 ± 0.24 were measured in the ETNP OMZ. In
107 agreement, Devol and Hartnett (2001) and Van Mooy et al. (2002) observed low particle
108 attenuation in the OMZ of the ETNP off Mexico, yielding *b* coefficients of 0.36 and 0.40,
109 respectively. Keil et al. (2015) found *b* values of 0.59-0.63 in the suboxic Arabian Sea. These
110 studies thus indicate that a greater proportion of the sinking POM escapes degradation while
111 sinking through suboxic waters. However, influence of oxygen on organic matter degradation
112 may vary between individual components. For instance, degradation of hydrolysable amino
113 acid under suboxic conditions was found to continue with the same rate as compared to oxic
114 conditions (Van Mooy et al. 2002; Pantoja et al. 2004), suggesting that anaerobic and micro-
115 aerobic bacteria preferentially utilize nitrogen-rich components.
116
117 So far, little is known on sinking POM flux attenuation in hypoxic waters (<60 μmol O_2 kg^{-1}),
118 which are more widespread (~4% of ocean volume) compared to suboxic waters (< 0.05% of
119 ocean volume). Laboratory studies indicated that particle aggregates sinking through hypoxic
120 waters can become suboxic within their interior due to oxygen diffusion limitation and evolve
121 microbial degradation processes typical for suboxic waters (Alldredge and Cohen, 1987;
122 Ploug et al., 1997; Stief et al., 2016). For example, at an ambient O_2 concentration of 60 μmol
123 kg^{-1}, the O_2 uptake by a 2 mm (diameter) aggregate was diffusion-limited and a 0.5 mm wide
124 anoxic core occurred within its interior (Ploug and Bergkvist, 2015). Since OMZs are
125 expected to expand in the future as a consequence of global warming and altered circulation
126 patterns (Stramma et al., 2008), the role of oxygen in controlling the biological pump
127 efficiency needs to be better constrained for predicting ocean-climate feedbacks. In order to
128 assess what controls carbon flux attenuation and depth-related changes in sinking particle
129 composition in hypoxic waters, we determined downward POM fluxes in the ETNA off the
130 coast of Mauritania, which exhibits an extensive hypoxic OMZ between 300 and 500 m. We
131 used two parallel drifting, surface-tethered sediment trap devices with particle interceptor

traps (PITs) at 7-8 different depths between 60-600 m to estimate fluxes to and within the OMZ.

2. Methods

2.1. The Study area

The study was conducted from March 17th to April 16th 2014 during a cruise of the RV METEOR to the ETNA region off the coast of Mauritania (Fig. 1a). The study area included hypoxic waters with minimum values of oxygen concentration of 40 µmol kg^{-1} as determined by CTD (Seabird) casts with two calibrated oxygen sensors at midwater depths of 350-500 m (Fig. 1b) (Visbeck, 2014).

2.2. Sediment trap operation and sample analysis

Free-drifting surface-tethered sediment trap devices were deployed for 196 h during the first deployment and 281h during the second deployment (Fig. 1c). The first trap device was deployed on the 24th of March 2014 (11:00 UTC) at 10.00°N 21.00°W with 12 Particle-Interceptor-Traps (PITs) at each of 8 depths: 60, 100, 150, 200, 300, 400, 500, and 600 m. The device was recovered on the 1st of April 2014 (14:30 UTC) at 10.46°N 21.39°W. The second device was deployed on the 27th of March 2014 (16:00 UTC) at 10.25°N 21°W with 12 PITs at each of 7 depths: 100, 150, 200, 300, 400, 500, and 600 m. The second trap device was recovered on the 8th of April 2014 (09:00 UTC) at 10.63°N 21.50°W. Both devices slowly drifted northwest and were recovered approximately 37 nm away from their deployment location (Fig. 1c). Within the drifting area oxygen concentration in the OMZ resembled the overall pattern of the Mauritanian upwelling with fully hypoxic conditions between 300 and 500 m (Fig. 1d).

157 The design of the trap devices and the drifting array basically follows Knauer et al. (1979),
158 with 12 PITs mounted on a polyvinylchloride (PVC) cross frame. The PITs were acrylic tubes
159 with an inside diameter of 7 cm, an outside diameter of 7.6 cm and a height of 53 cm, leading
160 to an aspect ratio of 7.5. The aspect ratio and a baffle system consisting of smaller acrylic
161 tubes attached to the top end of each PIT help to reduce drag-induced movement within the
162 trap (Soutar et al., 1977). PVC crosses with PITs were attached to a free-floating line, which
163 was buoyed at the surface and weighed at the bottom. The surface buoys of the arrays carried
164 GPS/Iridium devices and flashlights.
165 Prior to each deployment, each PIT was filled with 1.5 L filtered surface seawater (0.2 µm
166 pore size cartridge) collected from the ship's underway seawater system, up to 3/4 of the
167 PITs' height. A brine solution was prepared by dissolving 50 g L^{-1} sodium chloride with
168 filtered surface seawater and subsequently filtered through a 0.2 µm cartridge to remove
169 excess particulates. 20 ml of formalin was then added per L of the solution to achieve a brine
170 solution with 2% formalin. The preservative solution was then slowly transferred into each
171 PIT beneath the 1.5 L of filtered seawater using a peristaltic pump. PITs were covered with
172 lids immediately, to minimize contamination before deployment.
173 Sample treatment after trap recovery followed recommendations given by Buesseler et al.
174 (2007b). After recovery, all PITs were capped to minimize contamination. The density
175 gradient was visually inspected and found intact at the position of prior to deployment or at a
176 maximum 2 cm above. Then, seawater was pumped out of each PIT using a peristaltic pump
177 down to 2-3 cm above the density gradient. The remaining ~0.6 L were subsequently
178 transferred to canisters, pooled from 11 tubes per depth. 40 ml formalin were added to each
179 canister. Samples from each depth were passed through a 500 µm nylon mesh. Swimmers
180 were removed from the mesh with forceps under a binocular microscope and the remaining
181 particles, which stuck to the mesh, were transferred back to the sample. Samples were
182 subsequently split into aliquots of the total sample. Therefore, the pooled sample was

transferred into a round 10 L canister and stirred at medium velocity with a magnetic bar. Aliquots were transferred into 0.5 L Nalgene bottles with a flexible tube using a peristaltic pump. Aliquots of samples were filtered under low pressure (<200 mbar) onto different filter types (combusted GF/F 0.7 μm, polycarbonate 0.4 μm, or cellulose acetate 0.8 μm; see below) for different analyses and stored frozen (-20 °C) until analyses.

2.2.1. Biogeochemical Analyses

The following parameters were determined: Total particulate mass (TPM), particulate organic carbon (POC), particulate nitrogen (PN), particulate organic phosphorus (POP), biogenic silica (BSi), chlorophyll *a* (Chl *a*), particulate hydrolysable amino acids (PHAA) and transparent exopolymer particles (TEP).

TPM was analyzed in triplicate. The following aliquots were filtered in triplicate onto pre-weighed 0.4 μm polycarbonate filters: 800 ml (2 x 400 ml; 8 % of total sample) for the depths of 600 m to 300 m of deployment #1, 400 ml (4 % of total sample) for the depths of 200 m and 150 m of deployment #1 and for all depths of deployment #2, 420 ml (4 % of total sample) for the depth of 100 m and 60 m of deployment #1. Filters were rinsed two times with Milli-Q water, dried at 60°C for 4 h and stored until weight measurement on a Mettler Toledo XP2U microbalance.

POC and PN aliquots were filtered in triplicate onto combusted (8h at 500°C) GF/F filters (Whatmann, 25 mm): 400 ml (4 % of total sample) for the depths of 600 m to 150 m of deployment #1, 420 ml (4 % of total sample) for the depths of 100 m and 60 m of deployment #1, 100 ml (1 % of total sample) for all depths of deployment #2. For the depths of 150 m, 100 m and 60 m of deployment #1, 400 - 420 ml (4 % of total sample) was filtered onto two filters, due to the high particle load at these depths. Filters were exposed to fuming

hydrochloric acid in a fuming box over night to remove carbonate and subsequently dried (60°C, 12 h). For analysis, the filters were enclosed in tin cups and analysed using an Euro EA elemental analyzer calibrated with an acetanilide standard. For the depths of 150, 100 and 60 m of deployment #1 the sum of both filters was taken.

POP was determined in triplicate, except for 60 m depth of deployment #1, which was only determined in duplicate. The following aliquots were filtered onto combusted GF/F filters (Whatmann, 25 mm): 400 ml (4 % of total sample) for the depths of 600 m to 150 m of deployment #1, 420 ml (4 % of total sample) for the depths of 100 m and 60 m of deployment #1, 100 ml (1 % of total sample) for all depths of deployment #2. For the depths of 200 m to 60 m of deployment #1, the volume of 400 ml/ 420 ml (4 % of total sample) was filtered onto two filters, due to the high particle load at these shallower depths. Organic phosphorus collected on the filters was digested in the potassium peroxydisulphate-containing substance Oxisolv (Merck) for 30 min in a pressure cooker and measured colorimetrically as ortho-phosphate following the method of Hansen and Koroleff (1999).

PHAA were determined in duplicate. The following aliquots were filtered onto combusted GF/F filters (25 mm): 400 ml (4 % of total sample) for the depths of 600 m to 150 m of deployment #1, 420 ml (4 % of total sample) for the depths of 100 m and 60 m of deployment #1, 100 ml (1 % of total sample) for all depths of deployment #2. For the depths of 150 m, 100 m and 60 m of deployment #1, the volume of 400 ml / 420 ml (4 % of total sample) was filtered onto two filters, due to the high particle load at these shallower depths. PHAA analysis was performed according to Lindroth & Mopper (1979) and Dittmar et al. (2009) with some modifications. Duplicate samples were hydrolyzed for 20 h at 100°C with hydrochloric acid (30%, Suprapur, Merck) and neutralized by acid evaporation under vacuum in a microwave at 60°C. Samples were washed with water to remove remaining acid.

Analysis was performed on a 1260 HPLC system (Agilent). Thirteen different amino acids were separated with a C18 column (Phenomenex Kinetex, 2.6 µm, 150 x 4.6 mm) after in-line derivatization with o-phtaldialdehyde and mercaptoethanol. The following standard amino acids were used: aspartic acid (AsX), glutamic acid (GlX), histidine (His), serine (Ser), arginine (Arg), glycine (Gly), threonine (Thr), alanine (Ala), tyrosine (Tyr), valine (Val), phenylalanine (Phe), isoleucine (Ileu), leucine (Leu), γ- amino butyric acid (GABA). α-amino butyric acid was used as an internal standard to account for losses during handling. Solvent A was 5% acetonitrile (LiChrosolv, Merck, HPLC gradient grade) in sodiumdihydrogenphospate (Merck, suprapur) buffer (pH 7.0), Solvent B was acetonitrile. A gradient was run from 100% solvent A to 78% solvent A in 50 minutes. The detection limit for individual amino acids was 2 nmol monomer L^{-1}. The precision was <5%, estimated as the standard deviation of replicate measurements divided by the mean. The degradation index (DI) was calculated from the amino acid composition following Dauwe et al. (1999).

BSi was determined in triplicate. The following aliquots were filtered onto cellulose acetate filters (0.8 µm): 400 ml (4 % of total sample) for the depths of 600 m to 150 m of deployment #1, 420 ml (4 % of total sample) for the depths of 100 m and 60 m of deployment #1, 200 ml (2 x 100 ml; 2 % of total sample) for all depths of deployment #2. Filters were incubated with 25 ml NaOH (0.1 M) at 85˚C for 2h 15min in a shaking water bath. After cooling of the samples, analysis was conducted according to the method for determination of $Si(OH)_4$ by Hansen and Koroleff (1999). Fluxes of biogenic opal were calculated assuming a water content of ~10% and therefore the chemical formula SiO_2 x $0.4H_2O$ with a density of ~2.1 g cm^{-3} (Mortlock and Fröhlich 1989).

Chl *a* was determined in duplicate. The following aliquots were filtered onto GF/F filters (25 mm): 400 ml (4 % of total sample) for the depths of 600 m to 150 m of deployment #1, 420

ml (4 % of total sample) for the depths of 100 m and 60 m of deployment #1, 100 ml (1 % of total sample) for all depths of deployment #2. For the depths of 200 m to 60 m of deployment #1, the volume of 400 ml / 420 ml (4 % of total sample) was filtered onto two filters, due to the high particle load at these shallower depths. Samples were analyzed after extraction with 10ml of acetone (90%) on a Turner fluorimeter after Welschmeyer (1994). Calibration of the instrument was conducted with spinach extract standard (Sigma Aldrich).

TEP were determined in quadruplet by microscopy after Engel (2009). Between 3.5 and 10 ml (0.03-0.1% of total sample) for the depths of deployment #1 and #2 were filtered onto 0.4 µm Nuclepore membrane filters (Whatmann) and stained with 1 mL Alcian Blue solution. Filters were mounted onto Cytoclear© slides and stored at -20 °C until microscopy analysis using a light microscope (Zeiss Axio Scope A.1) connected to a camera (AxioCAM Mrc). Filters were screened at 200x magnification. 30 pictures were taken randomly from each filter in two perpendicular cross sections (15 pictures each; resolution 1040 x 1040 pixel, 8-bit color depth). Image analysis software WCIF ImageJ (Version 1.44, Public Domain, developed at the US National Institutes of Health, courtesy of Wayne Rasband, National Institute of Mental Health, Bethesda, Maryland) was used to semi-automatically analyse particle numbers and area.

The carbon content of TEP (TEP-C) was estimated after Mari (1999) using the size dependent relationship:

$$\text{TEP-C} = a \, \Sigma_i \, (n_i \, r_i^D), \qquad (1)$$

with n_i being the number of TEP in the size class i and r_i the mean equivalent spherical radius of the size class. The constant $a = 0.25 * 10^{-6}$ (µg C) and the fractal dimension of aggregates

D= 2.55 were proposed by Mari (1999). TEP-C was only calculated for the size fraction <5 µm including mainly free TEP, because larger TEP included TEP covered aggregates with solid particles. Estimating carbon content of these larger particles would overestimate TEP-C as the volume of the other particles would be included.

2.3. Calculations and statistics

Fluxes of $CaCO_3$ and lithogenic matter (lith) were calculated as:

$$[CaCO_3 + lith] = [TPM]-[POM]-[Opal], \quad (2)$$

Total mineral ballast ($ballast_{total}$) was calculated as:

$$[ballast_{total}] = [TPM]-[POM], \quad (3)$$

and the percentage of $ballast_{total}$ ($\%ballast_{total}$) was calculated as:

$$[\%ballast_{total}] = ([TPM] - [POM])/[TPM]*100, \quad (4)$$

The transfer efficiency (T_{eff}) of particulate components was calculated as the ratio of fluxes at 600 m to those at 100 m.

Calculated mean values include replicate measurements of both deployments. Data fits and statistical tests were performed with the software packages Microsoft Office Excel 2010, Sigma Plot 12.0 (Systat) and Ocean Data View (ODV) (Schlitzer, 2013). Weighted-average gridding was used in ODV to display data according to data coverage with automatic scale lengths. The overall significance level was $p<0.05$.

3. Results and Discussion

3.1. Fluxes of different compounds

Export fluxes of TPM and particulate organic elements determined during both trap deployments showed good overall agreement and a decrease with depth, fitting well to the power law function of *M87* (Fig. 2a-d, Fig.3a-d and Table 1). Averaging fluxes from both deployments yielded a total mass flux of 240 ± 34 mg m^{-2} d^{-1} at 100 m decreasing to 141 ± 8.8 mg m^{-2} d^{-1} in the core of the OMZ (400 m) (Fig. 2a). Fluxes of POC, PN and POP at 100 m depth were 73 ± 8.8, 13± 1.4 and 0.67 ± 0.06 mg m^{-2} d^{-1}, respectively, and decreased to 26 ± 4.5, 3.0 ± 0.41 and 0.19 ± 0.04 mg m^{-2} d^{-1} at 400 m depth (Fig. 2b-d). The contribution of POC flux to total mass flux (% OC) decreased from about 30% at 60-150 m depth to 17-20% at 400 m depth and showed only a minor decrease below 400 m, to 14-16% at 600 m depth. Similarly, the percentage of PN flux to total mass flux (% N) showed the largest decrease between 60 and 400 m, i.e. from 6.6% to 2.0-2.3%, and less decline below, reaching 1.7-1.8% at 600 m. The percentage of POP flux to total mass flux (% P) decreased from 0.37% at 60 m depth to 0.11-0.16% at 400 m depth, and remained constant below 400 m depth. No previous data are available for POM export fluxes at our study site for direct comparison. However, our trap data compare well to carbon export fluxes estimated from particle size data (i.e. 10-300 mg C m^{-2} d^{-1}) reported for 100 m depth in the area off Cape Blanc (Mauritania) by Iversen et al. (2010).

Fluxes of phytoplankton biomass, as indicated from Chl *a*, were similar at 100 m during both deployments, with 104 ± 1.5 µg Chl *a* m^{-2} d^{-1} during the first and 116 ± 6.2 µg m^{-2} d^{-1} during the second deployment, but behaved differently below, with a stronger flux attenuation above

339 the OMZ during the first compared to the second deployment (Fig. 3a). Fluxes within the
340 OMZ core were 35 ± 0.1 µg m^{-2} d^{-1} (#1) and 53 ± 0.5 µg m^{-2} d^{-1} (#2) respectively.
341
342 Opal fluxes were also similar during both deployments, yielding an average of 47 ± 3.6 mg m^{-2}
343 d^{-1} at 100 m, steadily decreasing to 32 ± 2.4 mg m^{-2} d^{-1} at 400 m depth (Fig. 3b). Similar to
344 Chl *a*, opal fluxes were slightly higher above the OMZ during the second compared to the
345 first deployment, but quite similar or even lower below the OMZ. This may indicate that the
346 second trap device, which drifted more northerly (Fig. 1c), exploited waters of a more recent
347 diatom bloom compared to the first deployment.
348 Fluxes of [$CaCO_3$ + lith] were similar to opal fluxes during the first deployment (F_{100}=52 mg
349 m^{-2} d^{-1}) but considerably lower during the second (F_{100}=14.8 mg m^{-2} d^{-1}) (data not shown).
350
351 During this study, export fluxes of TEP were estimated from decrease over depth of total
352 particle area and showed the strongest depth attenuation between 60 and 100 m during the
353 first deployment (Fig. 3c). Like Chl *a* fluxes, TEP export fluxes were slightly higher during
354 the second compared to the first deployment. At 100 m depth, average TEP flux was 1860 ±
355 46 cm^2 m^{-2} d^{-1} and decreased to 1190 ± 52 cm^2 m^{-2} d^{-1} at 400 m. Using a TEP size to carbon
356 conversion according to Mari (1999) yielded to an average TEP-C (<5 µm) flux of 1.73 ±
357 0.35 mg C m^{-2} d^{-1} at 100m depth, slightly decreasing to 1.64 ± 0.28 mg m^{-2} d^{-1} at 400 m and
358 further to 0.90 ± 0.32 mg m^{-2} d^{-1} at 600 m. Although TEP supposedly play an important role
359 in particle export fluxes (Passow, 2002; Arrigo, 2007; Chow et al., 2015), only a few previous
360 estimates for TEP export fluxes based on sediment traps have been given so far to which we
361 can compare our data. Martin et al. (2011) measured TEP export fluxes during a spring
362 bloom in the Iceland Basin (Northeast Atlantic Ocean) using the PELAGRA neutrally
363 buoyant sediment traps and determined values in the range of 30-120 mg Gum Xanthan
364 Equivalent m^{-2} d^{-1}. Ebersbach et al. (2014) obtained lower values of 0.03-5.14 mg Gum

Xanthan Equivalent m^{-2} d^{-1} during the LOHAFEX iron fertilization experiment in the Southern Ocean. Assuming a conversion factor of 0.63 µg C $µg^{-1}$ Gum Xanthan after Engel (2004), these previous estimates suggest TEP-C export fluxes ranging from 0.02 to 3 mg m^{-2} d^{-1} for the Southern Ocean and from 19 to75 mg m^{-2} d^{-1} for the North Atlantic spring bloom. Our data on TEP export fluxes for ETNA region are within the range of these previous studies, but closer to the lower estimates for the Southern Ocean. It has to be emphasized, though, that our calculated TEP-C fluxes are likely underestimates, since only suspended, i.e. 'free' TEP < 5 µm were taken into account. TEP-C associated to aggregates cannot be determined with the applied microscopic technique. Overall, TEP-C export fluxes in the ETNA were significantly related to Chl *a* fluxes, yielding [TEP-C, mg m^{-2} d^{-1}] = 11.9 [Chl *a*; mg m^{-2} d^{-1}] + 0.74 (r^2=0.59, n= 15, p<0.01).

A strong decrease at shallow depth (60–100 m) was also observed for PHAA fluxes during the first deployment (Fig. 3d). Average PHAA fluxes were 330 ± 51 µmol m^{-2} d^{-1} at 100 m, and 90 ± 20 µmol m^{-2} d^{-1} in the OMZ core at 400 m. These fluxes are equivalent to amino acid related fluxes of 16.8 ± 2.6 mg C m^{-2} d^{-1} (100 m) and 4.48± 1.0 mg C m^{-2} d^{-1} (400 m), respectively, which are typical values for PHAA-C fluxes in the ocean (Lee and Cronin, 1984). PHAA fluxes decreased slightly within the OMZ, i.e. from 300 to 500 m.

3.2. Flux attenuation in the ETNA OMZ

Fluxes from both deployments were fitted to the exponential decrease model (Martin et al., 1987) and attenuation coefficients (*b*-values) were estimated for all components (table 1). Higher *b*-values suggest stronger attenuation and may hint to either reduced sinking velocities of particles or to faster degradation of more labile components. During this study, PHAA were the most rapidly attenuated components of sinking particles, followed by POP, PN,

391 POC, Chl *a*, and TEP (table 1). Attenuation of mineral fluxes was less pronounced than for
392 TPM.
393 Attenuation coefficient of POC export fluxes was 0.80 during the first and 0.74 during the
394 second deployment. These values are in the intermediate range of previously determined *b*-
395 values for POC attenuation in the mesopelagic, shown to vary between 0.51 as determined in
396 the North Pacific (K2) and 1.59 as determined for the NASG (Buesseler et al., 2007a; Marsay
397 et al., 2015). Based on trap data from fully oxygenated water columns, Marsay et al. (2015)
398 recently suggested a linear relationship between POC flux attenuation and median water
399 temperature within the upper 500m of the water column according to: $b=0.062T+0.303$.
400 Applying this relationship to our study area, with temperature decreasing from 26°C at the
401 surface to 9°C at 500 m and a median temperature value of 12.01°C, would give a *b*-value of
402 1.05. This estimated *b*-value is higher than the values observed in this study (0.74 - 0.80) and
403 suggests that oxygen deficiency may reduce attenuation of POC fluxes in the ETNA resulting
404 in higher T_{eff} of organic matter though the OMZ's compared to well oxygenated waters.
405
406 Differences in flux attenuation coefficients translate into different T_{eff} for individual
407 components, with PHAA being the least and TEP being the most efficiently exported organic
408 component (table 1). In particular, values of T_{eff} for TEP and therewith for TEP-C were about
409 three times higher than for PHAA-C and even clearly higher than for bulk POC, suggesting a
410 preferential export of carbon included in TEP below 100 m. However, a steep decrease of
411 TEP flux was observed between 60 m and 100 m during the first deployment. TEP are
412 produced by a variety of organisms, i.e. different phytoplankton and bacterial species and
413 cannot be considered as of homogenous composition. Several mechanisms may therefore be
414 responsible for a change in TEP transfer efficiency with depth: 1) change of TEP
415 degradability with depth, 2) differences in TEP composition over depth related to association
416 with particles of different settling speed, 3) new production of TEP, abiotically or by bacteria,

during solubilization and degradation of sinking particles, 4) capture of suspended TEP by sinking aggregates, or 5) reduced degradation rate of TEP at lower oxygen. In support of the latter hypothesis, an attenuation of TEP fluxes within the OMZ (300-500 m) was not detectable, but rather occurred again below the OMZ.

3.3. Changes in POM composition during export

POM, assumed to be 2.2 × [POC] following Klaas and Archer (2002) made the greatest contribution to TPM flux at 60 m, but decreased below. Conversely, [%ballast$_{total}$] increased with depth, namely from 30% w/w at 60 m to 68% w/w at 600 m.

Biogenic opal (density: 2.1 g cm^{-3}) in the ocean is produced mainly by diatoms and radiolarians. During this study, opal made a rather constant contribution to TPM fluxes with 20-25% weight below 100 m. Hence, the observed increase in the [%ballast$_{total}$] with depth was due to an increasing contribution of $CaCO_3$ and lithogenic material. [$CaCO_3$+ lith] to TPM increased from 10-15% above 150 m to 45% at 600 m. As a consequence, the ballast ratio, defined as [Opal]:[$CaCO_3$+lith] changed from a dominance of opal above the OMZ to a dominance [$CaCO_3$+lith] within and below the OMZ (Figure 4). Slight differences were observed between the two deployments. Contribution of opal and of [$CaCO_3$+lith] to TPM at 100m was almost equal during the first deployment with a share of 18% and 22%, respectively. During the second deployment the contribution of opal to TPM at 100 m was 21% but only 6% for [$CaCO_3$+lith]. Thus, the higher contribution of opal to TPM fluxes together with higher Chl *a* fluxes indicated that diatomaceous material had a higher share of particles sinking out of the euphotic zone down to the OMZ core during the second compared to the first deployment.

Molar [POC]:[PN] ratios were close to the Redfield ratio at depths shallower than 100 m, increased to a ratio of 10 at 400 m depth and remained constant between 400 and 600 m

443 depth (Fig. 5a). [PN]:[POP] ratios were much above Redfield, with values varying between
444 30 and 45 throughout the water column (Fig. 5b). Also [POC]:[POP] ratios were much higher
445 than Redfield ratios, and showed an increasing trend down to 300-400 m depth, while
446 decreasing below (Fig. 5c). These changes in elemental ratios suggested a preferential
447 remineralization of POP in the upper 300 m, followed by PN and POC deeper down.
448 The percentage of total organic matter in TPM fluxes decreased from 67% at 100m to 32% at
449 600m (Fig. 6d). As a consequence of higher T_{eff} of TEP relative to bulk POC, contribution of
450 TEP-C to POC increased significantly with depth during both deployments ($p<0.01$; $r^2=0.59$,
451 n=15) and was 2% at 100 m, and 6% within and 5% below the OMZ (Fig. 5e). Because TEP
452 do not sink by themselves their export to depth depends on their incorporation into settling
453 aggregates. In a laboratory study, Engel et al. (2009) observed that decomposition of TEP was
454 faster relative to bulk POC for aggregates formed from calcifying and non-calcifying
455 *Emiliania huxleyi* cultures. In that experiment, aggregate decomposition was investigated
456 under oxic conditions. Other studies also showed fast microbial degradation of TEP under
457 oxic conditions (Bar-Zeev and Rahav, 2015). One possible explanation for increasing [TEP-
458 C]:[POC] in the hypoxic OMZ of the ETNA region could be that TEP are mostly included in
459 sinking aggregates, whereas POC could be included in various particle types, such as large
460 cells, detritus or fecal pellets. Ploug et al. (1997) estimated that carbon turn-over time inside
461 anoxic aggregates can be strongly reduced. Due to high microbial activity and reduced water
462 exchange aggregates sinking into hypoxic waters are more likely to experience anoxic
463 conditions than individual particles (Ploug and Bergkvist, 2015). Thus, TEP settling into
464 hypoxic waters by aggregates may be exposed to anoxia, and therewith to reduced microbial
465 degradation, in consequence leading to a preferential TEP transfer through the OMZ. This
466 may also explain the decrease of [TEP-C]:[POC] ratios below the OMZ at 600 m water depth,
467 which was, however, only observed during the second deployment. Since PN was more

rapidly degraded than POC this also implied that the ratio of [PN]:[TEP-C] became lower with depth.

In contrast to [TEP-C]:[POC], values of [PHAA-C]:[POC] in POM fluxes declined during both deployments above the OMZ. However, in the core of the OMZ, at 400 m, [PHAA-C]:[POC] was higher than at 300 and 500 m (Fig. 5f); the same pattern was also observed for [PHAA-N]:[PN] (data not shown). A faster decline in PHAA in sinking particles mainly above but not within the OMZ is different to observations gained for more extensively oxygen-deficient to full anoxic waters of the Eastern Tropical south Pacific (ETSP), which suggested that PHAA are preferentially degraded under low oxygen conditions (Van Mooy et al., 2002). In those studies, total hydrolysable amino acid (THAA) degradation under anoxic conditions was found to continue with the same rate compared to oxic conditions, while degradation of non-amino acid compounds was found to slow down (Pantoja et al., 2004; Van Mooy et al., 2002). A preferential degradation of nitrogen-rich compounds over POC suggests that microbes degrading organic matter under strongly oxygen deficient conditions via denitrification preferentially utilize nitrogen-rich amino acids (Van Mooy et al., 2002). Our data on PHAA do not suggest preferential amino acid loss due to components of sinking POM degradation in the ETNA OMZ. This is in accordance with the absence of microbial N-loss processes/ absence of denitrifying bacteria in ETNA oxygen deficient waters (Löscher et al., 2016). Instead, a slight increase of [PHAA-C]:[POC] in the OMZ may point to higher protein production by bacterial growth as previously observed for mesopelagic waters (Lee and Cronin, 1982, 1984) and may be related to increased growth efficiency of bacteria experiencing low oxygen condition as suggested by Keil et al. (2016).

Among all amino acids determined, GlX, Gly, Gaba and Leu showed the most pronounced variations with depth (Fig. 6a-d, table 2). Whereas GlX and Leu showed a decrease with

depth (Fig. 6a, c), Gly continuously increased. It has been shown that Gly is enriched in the silica-protein complex of diatom frustules (Hecky et al., 1973). Preservation of frustules relative to POM may therefore explain the relative increase of Gly with depth in sinking particles. GlX has been used as a biomarker (Abramson et al., 2010), since GlX was shown to be enriched in calcerous plankton (Weiner and Erez, 1984). During this study %Mol of GlX was higher during the first deployment, which is in accordance with the observed higher contribution of [$CaCO_3$+lith] to TPM flux. Gaba has been used as an indicator for bacterial decomposition activity (Lee and Cronin, 1982; Dauwe and Middelburg, 1998; Engel et al., 2009). During this study %Mol Gaba behaved differently during the first compared to the second deployment with similar values within the OMZ, a pattern also observed for opal fluxes (Fig. 3b). Moreover, %Mol of Gaba showed a local peak at 300 m, i.e. within the upper oxycline, and may point to high bacterial activity at this depth. Leu is an essential amino acids and readily taken up by heterotrophic microorganisms. Little change in %Leu in the OMZ core (Fig. 3d) compared to above (<300 m) indicated reduced microbial reworking of organic matter under hypoxic conditions. Another indication of microbial reworking of organic matter can be derived from the Degradation index (DI) (Dauwe et al., 1999). During this study, the DI decreased with increasing depth, but with differences between the deployments (Fig. 7). During #2, DI was slightly higher above the OMZ indicating fresher material. During #1 DI did not decrease within the OMZ, but it continued to decrease from 300 m to 500 m depth during deployment #2. Together with observations on Chl *a* and opal fluxes, as well as changes in ballast ratio, data on DI suggest that the particles of more diatomaceous origin likely continued to decompose under hypoxic conditions.

4. Conclusions

519 Despite an improvement in understanding principle processes and drivers of particle export
520 processes over the past decades, spatial and temporal variability of export fluxes in the ocean
521 are still difficult to predict. This is partly due to the lack of observations in different regions
522 of the mesopelagic realm. Our study is the first to describe fluxes of POM in the hypoxic
523 mesopelagic waters of the ETNA. Our data suggest a higher transfer efficiency than expected
524 from seawater temperature solely, suggesting reduced degradation of organic matter by
525 heterotrophic communities at low oxygen concentration (<60 µmol O_2 kg^{-1}). The biological
526 carbon pump in high productivity regimes associated to OMZs, i.e. Eastern Boundary
527 Upwelling Systems such as the ETNA region off Mauritania, may therewith be more efficient
528 than in fully oxygenated waters of comparable temperature. In contrast to suboxic systems (<
529 5 µmol O_2 kg^{-1}) a relatively higher loss of amino acids from POM fluxes was not evident for
530 the hypoxic water-column, suggesting microbial N-loss processes were comparatively minor
531 within particles. This, however, requires further investigation since no corresponding rate
532 measurements of denitrification or anammox were conducted during this study. Organic
533 matter composition seems to have a large impact on transfer efficiencies as carbon fluxes
534 associated to amino acids were much more attenuated over depth than carbon fluxes
535 associated to polysaccharide-rich TEP. If these findings are transferable to other oceanic
536 regions, changes in surface ocean organic matter composition in response to climate change
537 may also impact the carbon remineralization depth and therewith may have a feed-back
538 potential to atmospheric CO_2 concentration that yet has to be assessed.
539
540 **5. Competing interest**
541 The authors declare that they have no conflict of interest.
542
543 **6. Acknowledgements**

This study is a contribution to the Collaborative Research Center 754 / SFB Sonderforschungsbereich 754 ‘Climate-Biogeochemistry Interactions in the Tropical Ocean’. We thank Martin Visbeck, Toste Tanhua, Tobias Hahn, Sunke Schmidtko, and Gerd Krahmann for scientific and technical support as well as for providing oxygen and CTD data. Many thanks go to the shipboard scientific party and crew of Meteor cruise M105. Jon Roa, Ruth Flerus, Scarlett Sett and Tania Klüver are acknowledged for technical assistance. We thank Cindy Lee (Stony Brook University) for helpful advices. FACLM is supported by the DFG Excellence cluster Future Ocean. All data will become available at www.pangea.de upon publication.

References

Abramson, L., Lee, C., Liu, Z.F., Wakeham, S.G., and Szlosek, J.: Exchange between suspended and sinking particles in the northwest Mediterranean as inferred from the organic composition of in situ pump and sediment trap samples. Limnol. Oceanogr., 55, 2, 725-739, doi: 10.4319/lo.2009.55.2.0725, 2010.

Alldredge, A. L. and Cohen, Y.: Can microscale chemical patches persist in the sea? Microelectrode study of marine snow, fecal pellets. Science, 235, 4789, 689-91, 1987.

Alldredge, A. L., and Gotschalk, C. C.: Direct observation of the mass flocculation of diatom blooms: characteristics, settling velocities and formation of diatom aggregates. Deep-Sea Research, 36, 159–171, 1989.

Alldredge, A. L., U. Passow, and Logan, B. E.: The abundance and significance of a class of large, transparent organic particles in the ocean. Deep-Sea Res. 40, 1131–1140, 1993.

Arrigo, K. R.: Carbon cycle - Marine manipulations. NATURE, 450, 7169, 491-492, 2007.

Azetsu-Scott, K., and Passow, U.: Ascending marine particles: Significance of transparent exopolymer particles (TEP) in the upper ocean. Limnol. Oceanogr. 49, 3, 741-748, 2004.

Bar-Zeev, E., and Rahav, E.: Microbial metabolism of transparent exopolymer particles during the summer months along a eutrophic estuary system. Frontiers in Microbiol. 6, 403, doi: 10.3389/fmicb.2015.00403, 2015.

581

582 Belcher, A., Iversen, M., Manno, C., Henson, S. A., Tarling, G. A., and Sanders, R.: The role
583 of particle associated microbes in remineralization of fecal pellets in the upper mesopelagic of
584 the Scotia Sea, Antarctica. Limnol. Oceanogr. 61, 3, 1049-1064, doi: 10.1002/lno.10269 ,
585 2016

586

587 Bishop, J. K. B., Ketten, D. K., and Edmon, J. M.: The chemistry, biology and vertical flux of
588 particulate organic matter from the upper 400 m of the Cape Basin in the southeast Atlantic
589 Ocean. Deep-Sea Res. 25, 1121-1161, 1978.

590

591 Buesseler, K. O.: The decoupling of production and particulate export in the surface ocean.
592 Global Biogeochem. Cycles 12:297-310, 1998.

593

594 Buesseler, K.O., C.H. Lamborg, P.W. Boyd, P.J. Lam, T.W. Trull, R.R. Bidigare, J.K.B.
595 Bishop, K.L. Casciotti, F. Dehairs, M. Elskens, M. Honda, D.M. Karl, D.A. Siegel, M.W.
596 Silver, D.K. Steinberg, J. Valdes, B. Van Mooy, and Wilson S.: Revisiting carbon flux
597 through the ocean's twilight zone. Science, 316, 567–570, 2007a

598

599 Buesseler, K.O., Antia, A., Chen, M., Fowler, S. W., Gardner, W.D., Gustafsson, O., Harada,
600 K., Michaels, A.F., van der Loeff, M. R., Sarin, M., Steinberg, D. K. and Trull, T.: An
601 assessment of the use of sediment traps for estimating upper ocean particle fluxes. Journal of
602 Marine Research, 65, 345-416, 2007b.

603

604 Buesseler, K.O., and Boyd P.W.: Shedding light on processes that control particle export and
605 flux attenuation in the twilight zone. Limnol. Oceanogr., 54, 4, 1210–1232, 2009

606

607 Cavan, E.L., Le Moigne, F. A. C., Poulton, A. J., Tarling, G. A., Ward, P., Daniels, C. J.,
608 Fragoso, G. M., and Sanders, R. J. : Attenuation of particulate organic carbon flux in the
609 Scotia Sea, Southern Ocean, is controlled by zooplankton fecal pellets. Geophys. Res. Lett.,
610 42, 3, 821-830, doi: 10.1002/2014GL062744, 2015
611
612 Chow, J. S., Lee, C. and Engel, A.: The influence of extracellular polysaccharides, growth
613 rate, and free coccoliths on the coagulation efficiency of *Emiliania huxleyi*. Mar. Chem., 175,
614 2015.
615
616 Dauwe, B., and Middelburg, J.J.: Amino acids and hexosamines as indicators of organic
617 matter degradation state in North Sea sediments. Limnol. Oceanogr. 43, 782-798, 1998.
618
619 Dauwe, B., Middelburg, J. J., Herman, P. M. J., and Heip, C. H. R.: Linking diagenetic
620 alteration of amino acids and bulk organic matter reactivity. Limnol. Oceanogr. 44, 1809–
621 1814, 1999.
622
623 Devol, A.H. and Hartnett, H. E.: Role of the oxygen minimum zone in transfer of organic
624 carbon to the deep ocean. Limnol. Oceanogr., 25, 1684-1690, 2001.
625
626 Dittmar, T., Cherrier, J., and Ludwichowski, K.-U.: The Analysis of Amino Acids in
627 Seawater. In: Practical Guidelines for the Analysis of Seawater, CRC Press, 2009.
628
629 Ebersbach, F., Assmy, P., Martin, P. et al.: Particle flux characterisation and sedimentation
630 patterns of protistan plankton during the iron fertilisation experiment LOHAFEX in the
631 Southern Ocean. Deep Sea Res. I, 89, 94-103, 2014.
632

633 Engel, A.: The role of transparent exopolymer particles (TEP) in the increase in apparent
634 particle stickiness (alpha) during the decline of a diatom bloom. J. Plankton Res., 22, 485-
635 497, 2000.
636
637 Engel, A.: Distribution of transparent exopolymer particles (TEP) in the northeast Atlantic
638 Ocean and their potential significance for aggregation processes Deep Sea Res. I:
639 Oceanographic Research Papers, 51, 1, 83-92, 2004.
640
641 Engel, A., Thoms, S., Riebesell, U., Rochelle-Newall, E. and Zondervan, I.: Polysaccharide
642 aggregation as a potential sink of marine dissolved organic carbon. Nature, 428, 929-932,
643 2004.
644
645 Engel, A., Abramson, L., Szlosek, J., Liu, Z., Stewart, G., Hirschberg, D. and Lee, C.:
646 Investigating the effect of ballasting by $CaCO_3$ in *Emiliania huxleyi*, II: Decomposition of
647 particulate organic matter. Deep-Sea Res. II, 56, 18, 1408-1419. DOI
648 10.1016/j.dsr2.2008.11.028, 2009.
649
650 Engel, A.: Determination of Marine Gel Particles, in: Practical Guidelines for the Analysis of
651 Seawater, edited, CRC Press, 2009.
652
653 Engel, A., Piontek, J., Grossart, H. P., Riebesell, U., Schulz, K. G. and Sperling, M.: Impact
654 of CO_2 enrichment on organic matter dynamics during nutrient induced coastal phytoplankton
655 blooms. J Plankton Res., 36, 3, 641-657. DOI 10.1093/plankt/fbt125, 2014.
656

Giering, S. L. C., Sanders, R., Lampitt, R. S.,, Anderson, T. A.,Tamburini, C., Boutrif, M., Zubkov, M. V., Marsay, C. M., Henson, S. A., Saw, K., Cook, K., and Mayor, D. J. Reconciliation of the carbon budget in the ocean's twilight zone. Nature, 507, 480-483, 2014.

Haake, B., Ittekkot, V., Ramaswamy, V., Nair, R. R., and Honjo, S. Fluxes of amino acids and hexosamines to the deep Arabian Sea, Mar. Chem., 40, 291–314, 1992.

Hansen, H.P, and Koroleff, F.: Determination of nutrients. In: Methods of seawater analysis. Grasshof, K. (ed), 159–228, 1999.

Hecky, R.E., Mopper, K., Kilham, P., and Degens, E. T.: Amino acid and sugar composition of diatom cell-walls. Mar. Biol., 19, 4, 323-331, doi: 10.1007/BF00348902, 1973.

Heinze, C., Meyer, S.,; Goris, N., Anderson, L., Steinfeldt, R., Chang, N., Le Quere, C., and Bakker, D. C. E. : The ocean carbon sink - impacts, vulnerabilities and challenges. Earth Syst. Dynamics, 6, 1, 327-358, doi: 10.5194/esd-6-327-2015, 2015.

Iversen, M. H., Nowald, N., Ploug, H., Jackson, G. A., and Fischer, G.: High resolution profiles of vertical particulate organic matter export off Cape Blanc, Mauritania: Degradation processes and ballasting effects. Deep-Sea Res., 57, 6, 771-784, doi:10.1016/j.dsr.2010.03.007, 2010.

Keil, R. G., Neibauer, J., Biladeau, C., van der Elst, K. and Devol A. H.: A multiproxy approach to understanding the "enhanced" flux of organic matter through the oxygen deficient waters of the Arabian Sea. Biogeosciences, 13, 2077-2092, 2016.

683 Klaas, C., and Archer, D. E.: Association of sinking organic matter with various types of
684 mineral ballast in the deep sea: Implications for the rain ratio. Global Biogeochem. Cycles,
685 16(4), 1116, doi:10.1029/2001GB001765, 2002.
686
687 Knauer, G.A., J.H. Martin, and Bruland, K.W.: Fluxes of particulate carbon, nitrogen, and
688 phosphorus in the upper water column of the northeast Pacific. Deep-Sea Research, 26, 97-
689 108, 1979.
690
691 Kohlfeld, K. E., and Ridgewell, A. Glacial-Interglacial Variability in Atmospheric CO2. In:
692 Surface Ocean–Lower Atmosphere Processes Geophysical Research Series, 187, American
693 Geophysical Union, doi:10.1029/2008GM000845, 2009.
694
695 Kwon, E. Y., Primeau, F., and Sarmiento J. L.: The impact of remineralization on the air-sea
696 carbon balance, Nat. Geosci., 2, doi:10.1038/ngeo612, 2009.
697
698 Lam, P. J, Doney, S. C. and Bishop J. K. B.: The dynamic ocean biological pump: Insights
699 from a global compilation of particulate organic carbon, $CaCO_3$ and opal concentrations
700 profiles from the mesopelagic. Global Biogeochem. Cycles., 25, GB3009, doi:
701 10.1029/2010GB003868, 2011.
702
703 Lampitt, R. S., Noji, T. and Von Bodungen, B.: What happens to zooplankton fecal pellets-
704 implications for material flux. Mar. Biol., 104, 1, 15-23, doi: 10.1007/BF01313152, 1990.
705
706 Le Moigne F., Sanders, R., Villa, M., Martin, A., Pabortsava, K., Planquette, H., Morris, P.
707 J. and Thomalla, S.. On the proportion of ballast vs non-ballast associated sinking POC in the
708 surface ocean. Geophys. Res. Letter. doi:10.1029/2012GL052980, 2012,

Lee, C., and Cronin, C.: The vertical flux of particulate nitrogen in the sea: Decomposition of amino acids in the Peru upwelling area and the equatorial Atlantic. J. Mar. Res. 40, 227-251, 1982.

Lee, C., and Cronin, C., Particulate amino acids in the sea: Effects of primary productivity and biological decomposition. Journal of Marine Research 42, 1075-1097, 1984.

Lindroth, P., and Mopper, K.: High performance liquid chromatographic determination of subpicomole amounts of amino acids by precolumn fluorescence derivatization with o-phthaldialdehyde, Analytical Chemistry, 51(11), 1667-1674, 1979.

Löscher, C., Bange, H. W., Schmitz, R. A., Callbeck, C. M., Engel, A., Hauss, H., Kanzow, T., Kiko, R., Lavik, G., Loginova, A. N., Melzner, F., Meyer, J., Neulinger, S. C., Pahlow, M., Riebesell, U., Schunck, H., Thomsen, S. and Wagner, H.: Water column biogeochemistry of oxygen minimum zones in the eastern tropical North Atlantic and eastern tropical South Pacific Oceans. Biogeosciences (BG), 13 . pp. 3585-3606. DOI 10.5194/bg-13-3585-2016, 2016.

Mari, X.: Carbon content and C:N ratio of transparent exopolymeric particles (TEP) produced by bubbling exudates of diatoms. Mar. Ecol. Progr. Ser., 183, 59-71, 1999.

Marsay, C. M., Sanders, R. J., Henson, S. S., Pabortsava, K., Achterberg, E. P., and Lampitt, R. S.: Attenuation of sinking particulate organic carbon flux through the mesopelagic ocean. Proc. Natl. Acad. Sci. U.S.A., 112, 4, 1089-1094, doi: 10.1073/ pnas.1415311112, 2015.

735 Martin, P., Lampitt, R. S., Perry, M. J. Sanders, R. Lee, C., and D'Asaro, E.: Export and
736 mesopelagic particle flux during a North Atlantic spring diatom bloom. Deep-Sea Research I
737 58, 338–349, 2011.
738
739 Martin, J.H., G.A. Knauer, D.M. Karl and Broenkow W.W.: Vertex – Carbon Cycling in the
740 Northeast Pacific. Deep-Sea Res. A, 34, 267-285, doi: 10.1016/0198-0149(87)90086-0, 1987.
741
742 Mortlock, R.A., and Froelich, P.N.: A simple method for the rapid determina- tion of biogenic
743 opal in pelagic marine sediments. Deep-Sea Res., Part A, 36, 1415– 1426, 1989.
744
745 Pantoja, S., Sepúlveda, J. and González H. E.: Decomposition of sinking proteinaceous
746 material during fall in the oxygen minimum zone off northern Chile. Deep Sea Research, I,
747 51, 55-70, 2004.
748
749 Passow, U.: Transparent exopolymer particles (TEP) in aquatic environments, Progress in
750 Oceanography, 55, 287-333, 2002.
751
752 Passow, U., Shipe, R. F., Pak, D. K., Brzezinski, M. A., & Alldredge, A. L.: Origin of
753 transparent exopolymer particles (TEP) and their role in the sedimentation of particulate
754 matter. Continental Shelf Research, 21, 327–346, 2000.
755
756 Ploug, H., Kühl M., Buchholz-Cleven, B., and Jørgensen, B.B.: Anoxic aggregates - an
757 ephemeral phenomenon in the pelagic environment? Aquat. Microb. Ecol., 13, 285–294,
758 1997.
759

760 Ploug, H., and Bergkvist, J.: Oxygen diffusion limitation and ammonium production within
761 sinking diatom aggregates under hypoxic and anoxic conditions. Mar. Chem. 176, 142-149,
762 2015.
763
764 Schlitzer, R., Ocean Data View, http://odv.awi.de, 2013.
765
766 Schneider, B., Engel, A., and Schlitzer, R.: Effects of depth- and CO2-dependent C:N ratios
767 of particulate organic matter (POM) on the marine carbon cycle. Global Biogeochemical
768 Cycles, 18, 2, doi:10.1029/2003GB002184, 2004.
769
770 Soutar, A., Kling, S. A., Crill, P. A., Duffrin, E., and Bruland K.W.: Monitoring the marine
771 environment through sedimentation. *Nature*, 266, 136-139, 1977.
772
773 Stief, P., Kamp, A., Thamdrup, B., and Glud, R.N. : Anaerobic Nitrogen Turnover by Sinking
774 Diatom Aggregates at Varying Ambient Oxygen Levels. Frontiers in Micriobiol., 7, 98 doi:
775 10.3389/fmicb.2016.00098, 2016.
776
777 Stramma, L., Johnson, G. C., Sprintall, J., and Mohrholz, V.: Expanding Oxygen-Minimum
778 Zones in the Tropical Oceans, Science, 320, 655-658, 2008.
779
780 Suess, E.: Particulate organic carbon flux in the oceans - surface productivity and oxygen
781 utilization, Nature 288, 260–263, 1980.
782
783 Torres Valdez, S., Painter, . C., Martin, A. P., Sanders, R. and Felden, J.: Data compilation of
784 fluxes of sedimenting material from sediment traps in the Atlantic Ocean. Earth system
785 Science Data, 6, 123-145, doi: 10.5194/essd-6-123-2014, 2014.

Van Mooy, B. A. S., Keil R. G., and Devol, A. H.: Impact of suboxia on sinking particulate organic carbon: Enhanced carbon flux and preferential degradation of amino acids via denitrification. Geochim. Cosmochim. Ac., 66, 457-465. doi: 10.1016/s0016-7037(01)00787, 2002.

Visbeck M.: Oxygen in the Tropical Atlantic OSTRE Second Tracer Survey – Cruise. No. M105 – March 17 – April 16, 2014 – Mindelo (Cape Verde) – Mindelo (Cape Verde). METEORBerichte, M105, 49 pp., DFG-Senatskommission für Ozeanographie, DOI:10.2312/cr_m105, 2014.

Volk, T., and Hoffert, M. I.: Ocean carbon pumps: Analysis of relative strengths and efficiencies in ocean driven atmospheric CO2 changes. In: Sundquist ET and Broecker WS (eds.) The Carbon Cycle and Atmospheric CO2: Natural Variations Archean to Present, Geophysical Monograph Series, vol. 32, pp. 99-110. Washington, DC: American Geophysical Union, 1985.

Weiner, S. and Erez, J.: Organic matrix of the shell of the foraminifer *Heterostegina depressa*. Journal of Foraminifera Res., 14, 3, 206-212, 1984.

Welschmeyer, N. A.: Fluometric analysis of chlorophyll a in the resence of chlorophyll b and pheopigments. Limnol. Oceanogr., 39, 1985-1992, 1994.

Tables

Table 1: Fluxes of particulate components at 100m depth (F_{100}) and in the core of the OMZ at 400m (F_{OMZ}), as well as the associated attenuation coefficients (*b*-values) and transfer

efficiencies (T_{eff}, %) over the depth range 100 to 600 m during two traps deployments in the ETNA. All units are in mg m^{-2} d^{-1} except for TEP fluxes which is reported in total particle area cm^{-2} m^{-2} d^{-1}. Mean values and standard deviations (SD) were calculated from analytical replicates.

Component		F_{100}		F_{OMZ}		*b-value*			T_{eff} *(%)*
		mean	SD	mean	SD	mean	SD	r^2	(600/100 m)
Mass	I	249	48.9	141	6.8	-0.429	0.090	0.987	41
	II	231	16.3	141	12.1	-0.355	0.033	0.998	52
POC	I	69.4	9.23	23.8	5.4	-0.795	0.031	0.989	23
	II	76.3	8.43	28.1	3.0	-0.741	0.044	0.989	22
PN	I	11.9	1.29	2.76	0.46	-1.013	0.026	0.992	15
	II	13.5	1.12	3.26	0.19	-1.00	0.020	0.990	16
POP	I	0.71	0.07	0.15	0.02	-1.081	0.074	0.992	18
	II	0.64	0.03	0.22	0.02	-0.80	0.034	0.990	23
Opal	I	44.6	1.76	34.0	1.7	-.0195	0.038	0.987	65
	II	48.6	4.16	30.7	2.0	-0.345	0.052	0.987	44
Chl *a*	I	0.10	0.00	0.035	0.001	-0.820	0.024	0.990	21
	II	0.12	0.01	0.053	0.005	-0.625	0.082	0.988	24
TEP	I	1650	548	119	36.8	-0.498	0.014	0.548	33
	II	2990	348	1644	95	-0.451	0.069	0.810	37
PHAA-C	I	3.21	-	3.71	0.47	-1.324	0.067	0.994	11
	II	1.28	0.10	5.24	0.79	-0.978	0.096	0.991	14

819 Table 2: Composition (%Mol) and degradation index (DI) of PHAA collected at different depths during two trap deployments (#I, #II) in the ETNA
820 region.

Depth(m)	AsX	GlX	Ser	Gly	Thr	Arg	Ala	GABA	Tyr	Val	Iso	Phe	Leu	DI
						#I								
60	14.15	13.94	8.46	14.29	7.76	5.90	11.94	0.22	0.84	5.69	4.57	4.00	8.26	0.34
100	13.95	13.53	8.29	14.65	7.87	5.77	11.57	0.19	1.64	5.66	4.56	4.07	8.24	0.23
150	14.19	12.73	8.54	15.93	8.10	5.78	11.42	0.31	0.96	5.68	4.44	4.05	7.87	0.29
200	14.17	12.05	9.29	16.02	8.05	5.61	11.69	0.49	1.10	5.65	4.30	4.04	7.54	0.07
300	13.19	11.75	8.58	17.71	7.98	5.31	12.10	0.37	1.82	5.77	4.15	3.83	7.43	0.03
400	14.15	11.77	9.03	18.54	7.94	5.72	10.85	0.46	1.25	5.58	3.93	3.80	6.97	0.02
500	14.06	11.89	9.55	18.70	7.18	6.01	11.02	0.55	1.29	5.19	3.86	3.65	7.05	0.02
600	14.15	13.94	8.46	14.29	7.76	5.90	11.94	0.22	0.84	5.69	4.57	4.00	8.26	0.07
						#II								
100	13.89	14.69	8.36	12.94	7.57	5.89	12.26	0.21	0.02	6.13	5.12	4.05	8.86	0.24
150	13.48	14.23	8.46	14.12	7.56	5.68	12.55	0.22	0.00	6.21	5.01	3.85	8.62	0.37
200	13.80	13.90	9.10	14.27	7.20	6.12	11.57	0.27	0.04	6.19	5.07	3.97	8.49	0.13
300	14.58	14.63	8.35	15.16	7.75	5.56	11.75	0.26	0.14	5.62	4.51	3.82	7.88	0.07
400	14.06	13.01	8.72	16.45	7.99	5.55	11.74	0.44	0.79	5.54	4.33	3.77	7.59	0.08
500	14.08	12.90	8.75	16.48	7.59	5.69	11.81	0.37	0.30	5.94	4.62	3.80	7.66	-0.09
600	13.62	12.55	9.16	17.02	7.95	5.75	11.23	0.42	0.38	5.87	4.61	3.88	7.55	-0.04

Figure captions:

Figure 1a-d: Map of the study area (A) and depth distribution of oxygen concentration (mol kg^{-1}) (B) in the Eastern Tropical North Atlantic (ETNA) during the RV Meteor 105 cruise, when two surface tethered drifting sediment traps (STDT) were deployed (C). Depth distribution of oxygen concentration (mol kg^{-1}) at stations visited in the deployment area showed an oxygen minimum zone in the upper mesopelagial (D).

Figure 2a-d: Fluxes of total mass (a) and particulate organic carbon (b; POC), particulate nitrogen (c; PN), and particulate organic phosphorus (d; POP) during the deployment of two STDT in the ETNA. Deployments: Solid symbols #I, open symbols #II.

Figure 3a-d: Fluxes of Chlorophyll *a* (a; Chl *a*), opal (b), TEP (c), and PHAA (d) during the deployment of two STDT in the ETNA. Deployments: Solid symbols #I, open symbols #II.

Figure 4: Changes in mineral ballast ratios of sinking particles with depth during the two deployments in the ETNA. Deployments: Black bars #I, grey bars #II.

Figure 5a-f: Changes in organic matter composition of particles sinking through the OMZ during the deployment of two STDT in the ETNA. Deployments: Solid symbols #I, open symbols #II.

Figure 6a-d: Molar percentages of selected amino acids contained in PHAA during the deployment of two STDT in the ETNA. Deployments: Solid symbols #I, open symbols #II.

Figure 7: Degradation index (DI) of organic matter in trap collected sinking particles based on amino acid composition and calculated after Dauwe et al. (1999). Deployments: Black bars #I, grey bars #II.

Figures

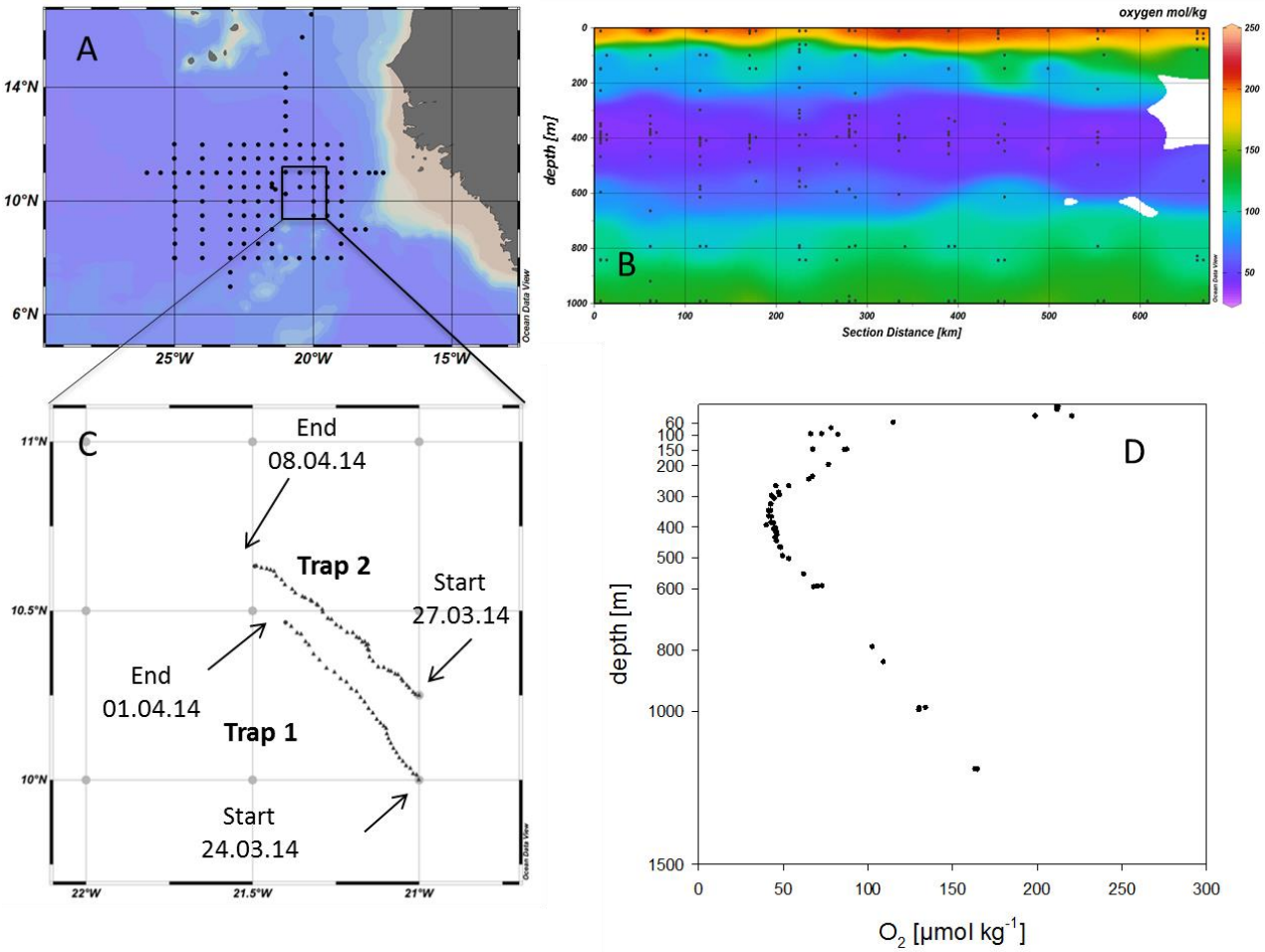

Figure 1a-d

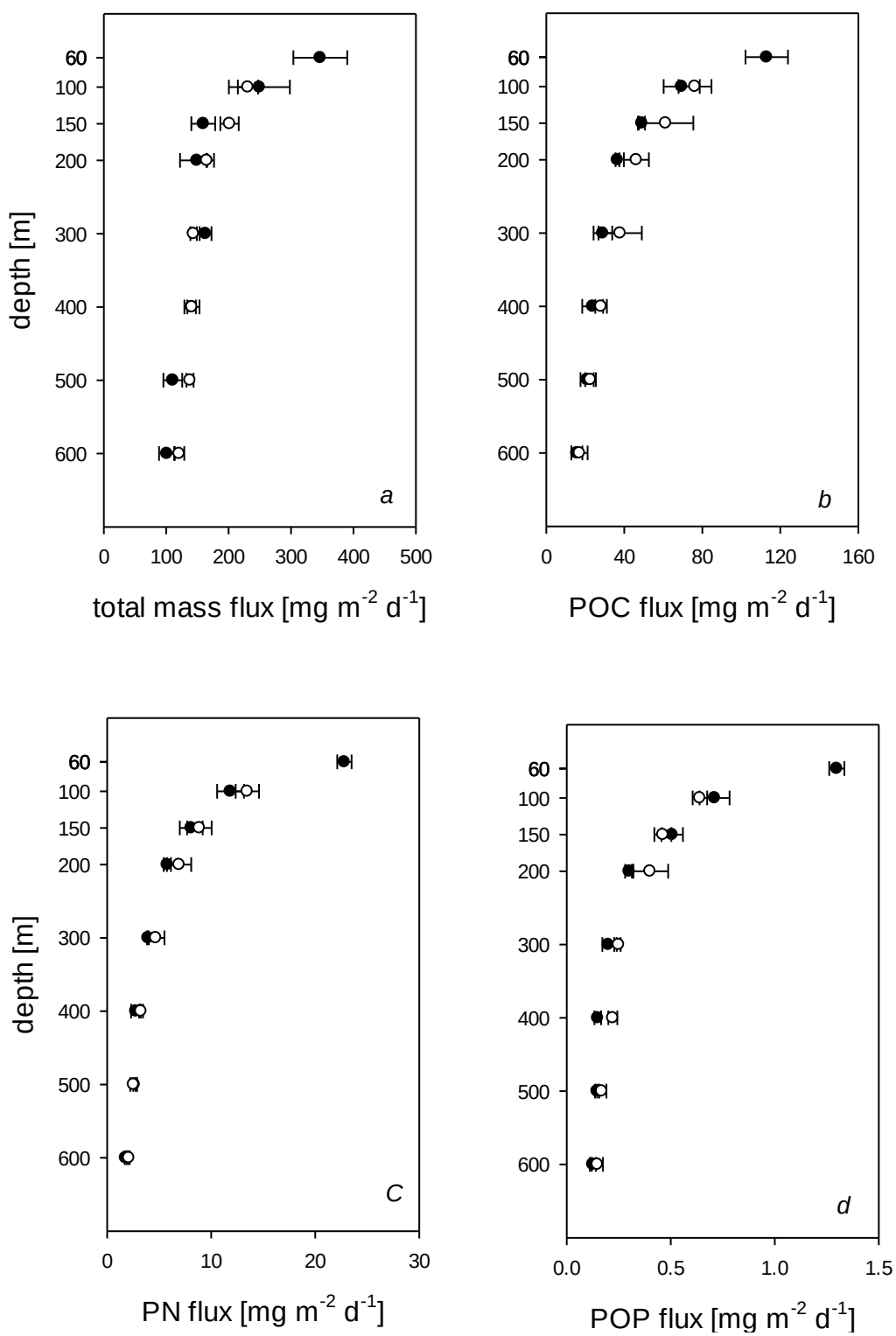
depth [m]
60
100
150
200
300
400
500
600
a
0
100
200
300
400
500
total mass flux [mg m-2 d-1]
b
0
40
80
120
160
POC flux [mg m-2 d-1]
C
0
10
20
30
PN flux [mg m-2 d-1]
d
0.0
0.5
1.0
1.5
POP flux [mg m-2 d-1]

Figure 2a-d

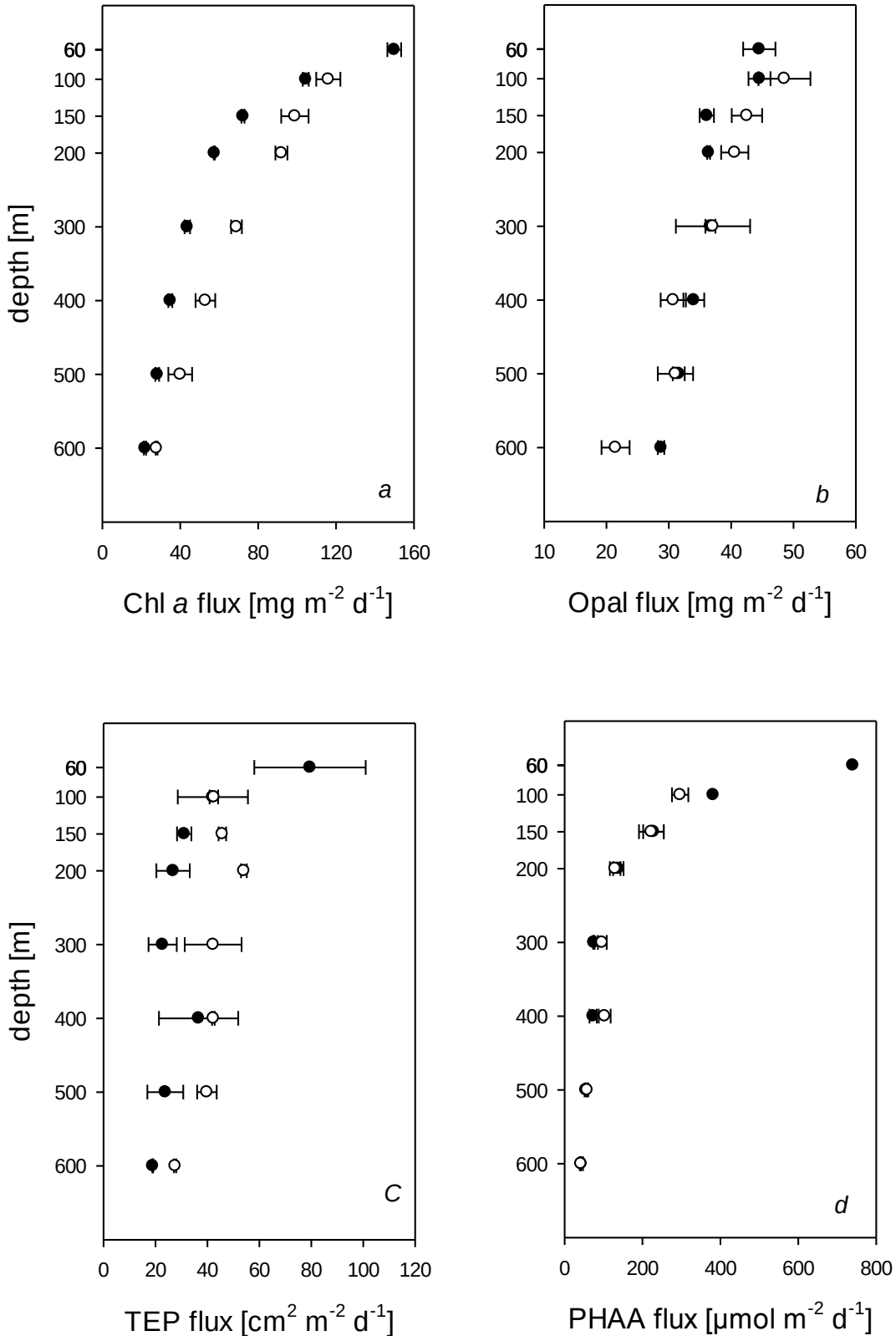
depth [m]
60
100
150
200
300
400
500
600
a
0
40
80
120
160
Chl a flux [mg m-2 d-1]
b
10
20
30
40
50
60
Opal flux [mg m-2 d-1]
C
0
20
40
60
80
100
120
TEP flux [cm2 m-2 d-1]
d
0
200
400
600
800
PHAA flux [µmol m-2 d-1]

Figure 3a-d

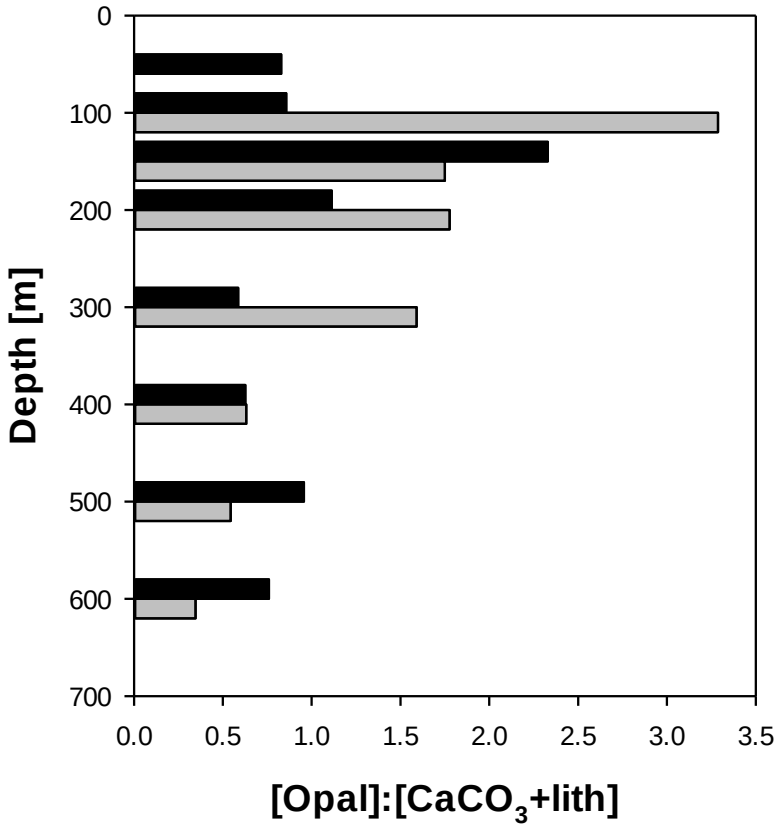
Depth [m]
0
100
200
300
400
500
600
700
0.0
0.5
1.0
1.5
2.0
2.5
3.0
3.5
[Opal]:[CaCO3+lith]

Figure 4

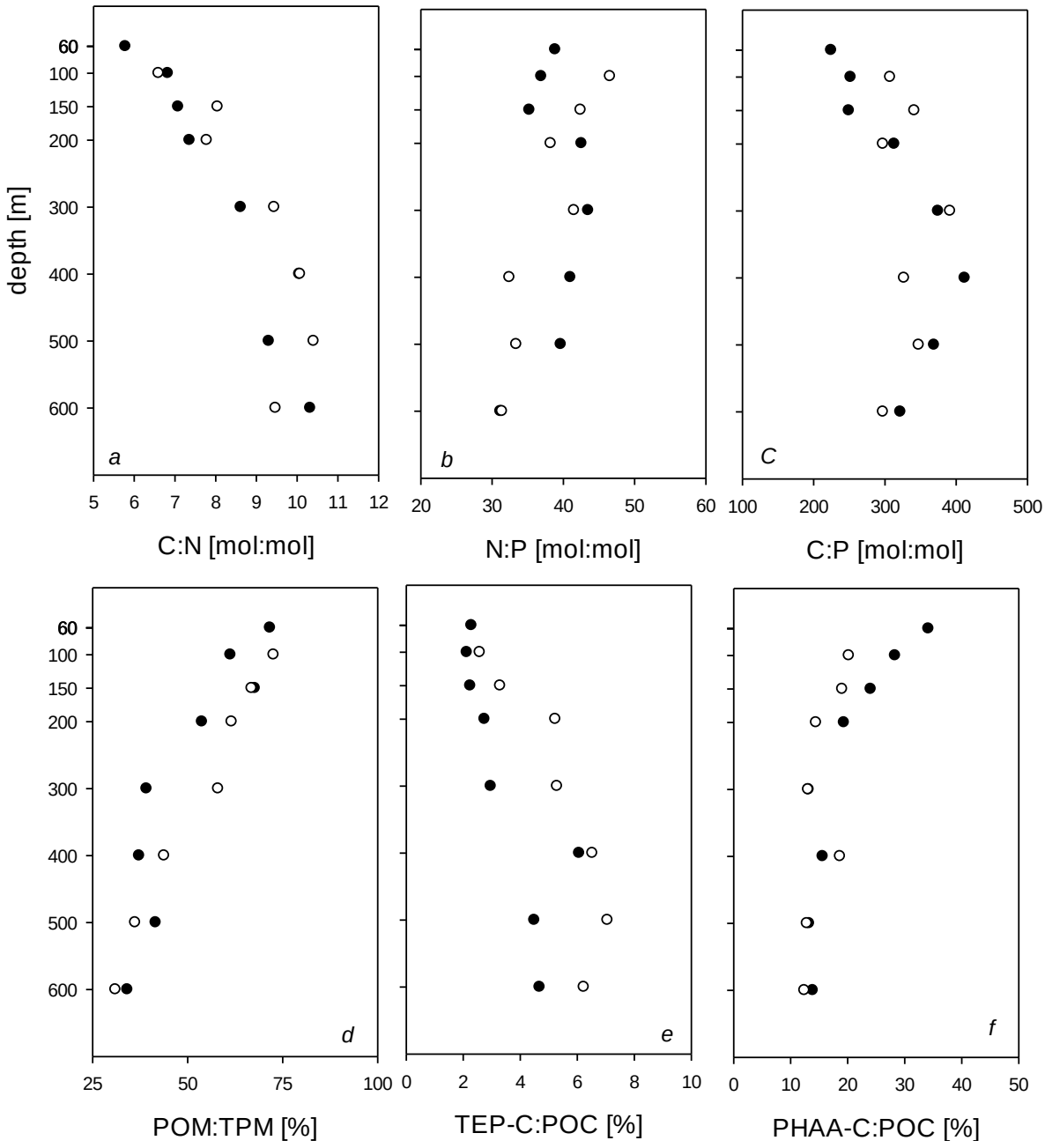
depth [m]
60
100
150
200
300
400
500
600
a
5 6 7 8 9 10 11 12
C:N [mol:mol]
b
20 30 40 50 60
N:P [mol:mol]
C
100 200 300 400 500
C:P [mol:mol]
d
25 50 75 100
POM:TPM [%]
e
0 2 4 6 8 10
TEP-C:POC [%]
f
0 10 20 30 40 50
PHAA-C:POC [%]

Figure 5a-f

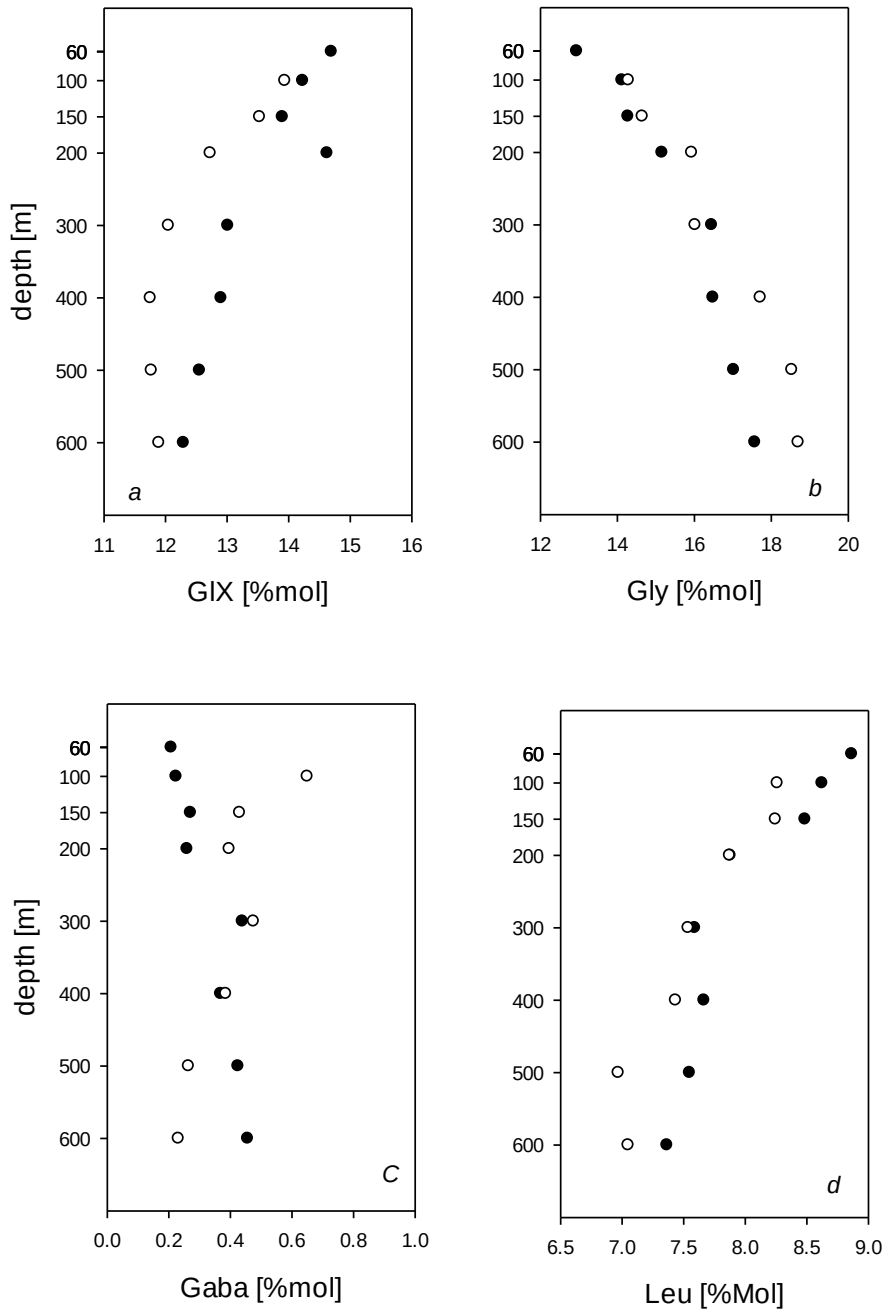
depth [m]
60
100
150
200
300
400
500
600
a
11
12
13
14
15
16
GIX [%mol]
b
12
14
16
18
20
Gly [%mol]
C
0.0
0.2
0.4
0.6
0.8
1.0
Gaba [%mol]
d
6.5
7.0
7.5
8.0
8.5
9.0
Leu [%Mol]

Figure 6a-d

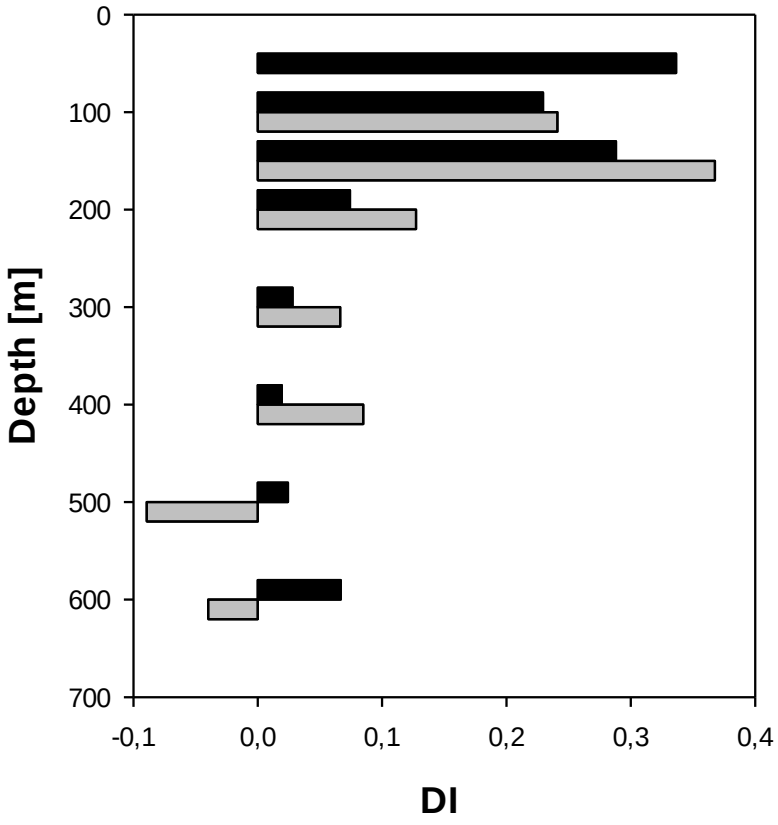

Figure 7